International Immunopharmacology 70 (2019) 125–134

Contents lists available at ScienceDirect

International Immunopharmacology

journal homepage: www.elsevier.com/locate/intimp

Modification of IL-24 by tumor penetrating peptide iRGD enhanced its antitumor efficacy against non-small cell lung cancer

Jie Yang[a,1], Jie Yang[a,b,1], Yanhong Wei[a,c,1], Hong Yin[a,b], Lin Fang[a], Dafei Chai[a], Huizhong Li[a], Hailong Li[a,d], Qing Zhang[a,*], Junnian Zheng[a,d,e,*]

[a] Cancer Institute, Xuzhou Medical University, Xuzhou 221002, China
[b] Center of Radiotherapy of The Second Affiliated Hospital of Xuzhou Medical University, Xuzhou 221002, China
[c] Center of Cancer of The Central Hospital of Yongzhou, Yongzhou 425000, China
[d] Center of Clinical Oncology, affiliated Hospital of Xuzhou Medical University, Xuzhou, Jiangsu 221002, China
[e] Jiangsu Center for the Collaboration and Innovation of Cancer Biotherapy, Cancer Institute, Xuzhou Medical University, Xuzhou 221002, China

ARTICLE INFO

Keywords:
iRGD
Interleukin-24
A549
Non-small cell lung cancer
Tumor-penetrating peptide

ABSTRACT

Interleukin-24 (IL-24) is known for its tumor suppressive activity and the selective induction of apoptosis of numerous human cancer cells, while demonstrating little harm to normal cells. However, poor tumor penetration remains a key problem for the efficacy of IL-24 as a treatment. The iRGD (CRGDK/RGPDC) is a novel tumor-specific peptide with unique tumor-penetrating and cell-internalizing properties. To enhance the tumor-penetrating effects of IL-24, the iRGD peptide was fused with the C-terminal domain of IL-24 to generate a novel recombinant protein, IL-24-iRGD. The aim of the present study was to investigate the antitumor effects of IL-24-iRGD in non-small cell lung cancer (NSCLC) cells *in vitro* and *in vivo*. It was observed that IL-24-iRGD increased the production of IL-6, TNF-α and INF-γ from human peripheral blood monocyte (PBMC), and suppressed cell growth of A549 *in vitro*. Then A549 cells were subcutaneously injected into nude mice, and these tumor-bearing mice were immunized with IL-24, IL-24-iRGD or PBS *via* the tail vein. The IL-24 and IL-24-iRGD-treated groups exhibited tumor growth inhibition rates of 26.2% and 59.1%, respectively, when compared with the PBS-treated group. Protein penetration into tumors was analyzed by immunofluorescence, cell apoptosis was examined by TdT-mediated dUTP nick end labeling, and the expression of cleaved caspase-3 was analyzed by immuno-histochemical staining. The results demonstrated that IL-24-iRGD induced apoptosis and inhibited the growth of A549 cells to a significantly greater extent when compared with IL-24 treatment alone. It may provide an improved strategy for antitumor therapy and the clinical treatment of NSCLC.

1. Introduction

In both sexes combined, lung cancer is the most frequently diagnosed cancer (11.6% of the total cases) and the leading cause of cancer death [1]. Lung cancer is also an increasing global health problem caused by air pollution, particularly in developing countries [2]. Non-small cell lung cancer (NSCLC) is the most common type of lung cancer, which accounts for ~75–80% of all lung cancer cases and exhibits high recurrence rates [3–5]. Chemotherapy and radiotherapy are the first line treatment options and the most common methods for the treatment of lung cancer; however, they are associated with serious side effects [6]. In addition, chemotherapy is limited by the low drug concentration at tumor sites and poor penetration into the parenchyma of solid tumors [6,7].

Interleukin-24 (IL-24) is a multi-faceted killer of various cancer cells [8,9]. It has shown significant clinical benefits in patients, and is well

Abbreviations: CCK-8, cell counting kit-8; DAB, diaminobenzidine; DAPI, 4′,6-diamidino-2-phenylindole; ELISA, enzyme-linked immunosorbent assay; FITC, fluorescein isothiocyanate; H&E, hematoxylin and eosin; HIV, human immunodeficiency virus; IFN-γ, interferon-γ; IgG, Immunoglobulin G; IL-24, interleukin-24; IOD, integrated optical density; IPTG, isopropyl-β-D-thiogalactoside; iRGD, CRGDK/RGPDC; McAb, monoclonal antibody; NRP-1, neuropilin-1; NSCLC, non-small cell lung cancer; OD, optical density; PBMC, human peripheral blood monocyte; PBS, phosphate-buffered saline; PBST, PBS + Tween 20; PE, phycoerythrin; PI, propidium iodide; RPMI, Roswell Park Memorial Institute; RT, room temperature; SD, standard deviation; SDS-PAGE, sodium dodecyl sulfate polyacrylamide gel electrophoresis; TNF-α, tumor necrosis factor-α; TUNEL, TdT-mediated dUTP nick end labeling

* Corresponding authors at: Cancer Institute, Xuzhou Medical University, 84 West Huai-hai Road, Xuzhou, Jiangsu 221002, China.
E-mail addresses: qingzhang@xzhmu.edu.cn (Q. Zhang), jnzheng@xzhmu.edu.cn (J. Zheng).
[1] These authors contributed equally.

https://doi.org/10.1016/j.intimp.2019.02.027
Received 9 October 2018; Received in revised form 14 February 2019; Accepted 14 February 2019
Available online 22 February 2019
1567-5769/

known for its tumor suppressive activity without damaging normal cells [9–11]. Previous studies have confirmed that IL-24 inhibits the migration and invasion of lung cancer cells, selectively inhibits cancer cell growth, and induces apoptosis [8,12]. However, the ineffective delivery of IL-24 to cancer cells hinders its extensive use.

Over the last few decades, tumor-targeting peptides have been a popular focus of research into cancer treatments [7,13]. Conventional RGD peptides bind selectively to integrins αvβ3 and αvβ5 [7,14] to successfully deliver drugs to the blood stream and slightly increase the accumulation of drugs at tumor sites [15]. However, the poor ability of RGD peptides to penetrate the tumor parenchyma remains a great challenge for cancer therapy [7].

iRGD (CRGDK/RGPDC) is a novel tumor-specific peptide with unique tumor-penetrating and cell-internalizing properties. It binds to integrins αvβ3 and αvβ5 and possesses the activity of binding to neuropilin-1 (NRP-1)-dependent cells [7,16]. Following the initial binding to αv integrins, iRGD is cleaved by proteases to expose the NRP-1 binding site, CRGDK/R, which effectively induces the process of tumor penetration [17]. It has been reported that intravenously injected compounds coupled to iRGD bind to tumor vessels and migrate into the extravascular tumor parenchyma with iRGD, thus increasing vascular and tissue permeability in a tumor-specific and NRP-1-dependent manner [17]. Due to this novel delivery system and low toxicity in normal cells, iRGD has become a particular focus of location for tumor imaging, diagnosis and preclinical research [3,6,18]. Chen et al. [19] reported that the treatment of tumor-bearing mice with iRGD conjugated to the cell death domain effectively inhibited tumor growth *in vivo*, and led to a ~80% reduction in MCF10CA1a tumor volume and a 40% reduction in 4T1 tumor volume [19]. In addition, Akashi et al. [20] reported a novel combination chemotherapy treatment involving gemcitabine in combination with the iRGD peptide, which enhanced tumor-specific drug penetration *via* the NRP-1 receptor. This indicated that NRP-1 overexpressing cancer models may be sensitive to iRGD [3].

In the present study, the iRGD peptide was fused with the C-terminal domain of IL-24 to generate a novel recombinant protein, termed IL-24-iRGD. The antitumor effects of IL-24-iRGD in NSCLC cells were then investigated *in vitro* and *in vivo*.

2. Materials and methods

2.1. Mice and cell lines

Male BALB/c nude mice (age, 5–6 weeks) were purchased from the Animal Center of Xuzhou Medical University (Xuzhou, China), and housed in the specific-pathogen-free animal facility of the Experimental Animal Center, Xuzhou Medical University. Mice were housed in a temperature (22 ± 1 °C)- and humidity (55 ± 5%)-controlled room with 12-h light/dark cycles, and allowed free access to sterile water and food. All cages housed up to 6 mice and contained wood shavings and an independent air supply system. All animal procedures performed complied with the guidelines approved by the Animal Research Committee at Xuzhou Medical University.

The A549 human lung cancer cell line and normal human lung fibroblasts NHLF were obtained from the cell bank of Chinese Academy of Science. A549 cells (Cell bank of Chinese Academy of Sciences, Shanghai, China) were maintained in RPMI −1640 medium supplemented with 10% heat-inactivated fetal calf serum and penicillin (100 U/ml)/streptomycin (100 mg/ml), while NHLF cells were maintained in Dulbecco's minimum essential medium (DMEM), (all reagents were supplied by Gibco; Thermo Fisher Scientific, Inc., Waltham, MA, USA) in a humidified atmosphere of 95% air and 5% CO_2 at 37 °C.

2.2. Construction of IL-24-iRGD plasmids

The gene sequence of iRGD encoding CRGDKGPDC was fused with C-terminus of IL-24, and the IL-24-iRGD gene sequence was amplified

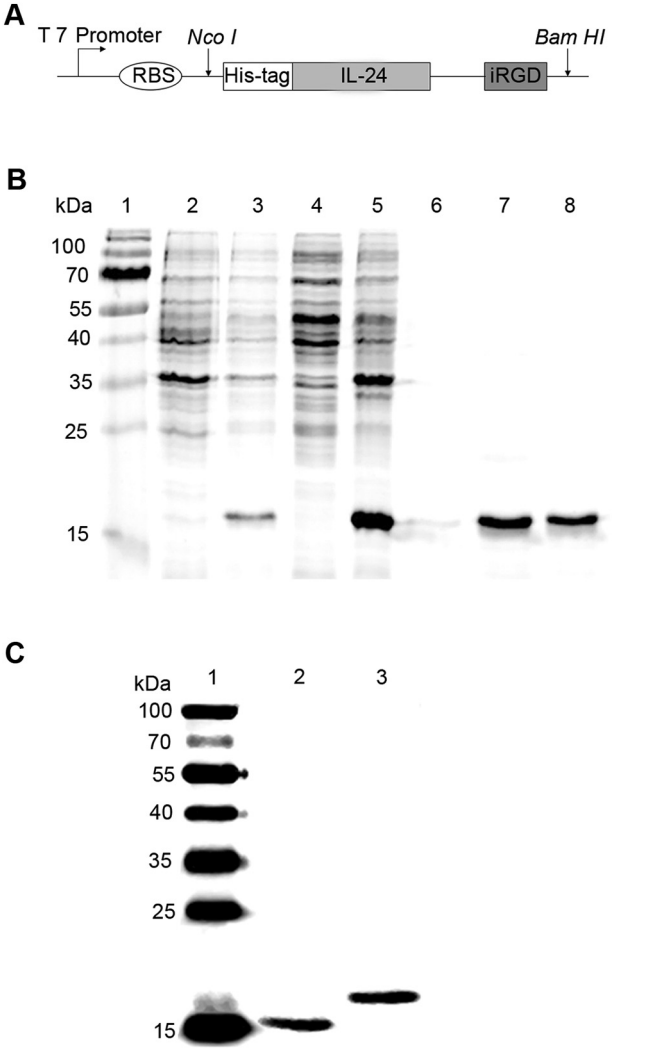

Fig. 1. Preparation of IL-24-iRGD. (A) A schematic of the pET19b-IL-24-iRGD expression vector. A His-tag was attached to the N-terminus of the IL-24 protein, while the iRGD peptide was attached to the C-terminus of the IL-24 protein by linker peptides. (B) 15% SDS-PAGE analysis of the expression and purification of IL-24-iRGD. Lane 1, molecular weight marker; lane 2, total cell protein from BL21 *E. coli* prior to IPTG induction; lane 3, total cell protein from BL21 *E. coli* induced by IPTG; lane 4, protein supernatant following lysis by ultrasonication; lane 5, protein precipitate following lysis; lanes 7–8, protein sample following purification by affinity chromatography. (C) Western blot analysis of IL-24 and IL-24-iRGD. Lane 1, molecular weight marker; lane 2, IL-24; lane 3, IL-24-iRGD. IL-24, interleukin-24; His, histidine; *E. coli*, *Escherichia coli*; IPTG, isopropyl-β-D-thiogalactoside.

by nested-polymerase chain reaction (PCR) using 4 oligonucleotide primers from the ZD55-IL-24 plasmid [21]. The sequences were as follows: S1, forward, 5′-CATG CCA TGG GC *CAT CAT CAT CAT CAT CAT CAT CAT CAT CAC* GCC CAG GGC CAA GAA TTC CAC TTT GG-3′ [underlined letters indicate the enzyme site of *Nco*I and italic letters represent the histidine (His)-tag]; S2, first reverse primer, 5′-CCA CTG CCG CCG CCG CCG CTA CCA CCA CCA CCG AGC TTG TAG AAT TTC-3′; S3, second reverse primer, 5′-GTC GCC GCG GCA AGA GCC ACC GCC ACC ACT GCC GCC GCC GCC-3′; S4, third reverse primer, 5′-CGC GGATCC TTA TTA *GCA GTC GGG GCC CTT GTC GCC GCG GCA* AGA GCC-3′ (italic letters represent the iRGD sequence, and the underlined letters (GGATCC) indicate the enzyme site of *Bam*HI). The thermal cycling protocol was as follows: 30 cycles of denaturation at 98 °C for 15 s, annealing at 55 °C for 5 s, and polymerization at 72 °C for 1 min, followed by a final polymerization step at 72 °C for 10 min. The PCR

product was digested with *Nco*I and *Bam*HI (Thermo Fisher Scientific, Inc.), purified, and cloned into the pET19b vector (maintained in our lab), which had been pre-digested with *Nco*I and *Bam*HI. The generated plasmid was named pET19b-IL-24-iRGD (Fig. 1A). All construct sequences were confirmed by DNA sequencing (Beijing Genomics Institute/BGI, Shanghai, China).

2.3. Expression and purification of IL-24-iRGD

The pET19b-IL-24-iRGD plasmid was transformed into the BL21 strain of *Escherichia coli* (*E. coli*). The bacteria were cultured in LB broth medium (Invitrogen; Thermo Fisher Scientific, Inc.) containing 50 μg/ml ampicillin (Sigma-Aldrich; Merck KGaA, Darmstadt, Germany) at 37 °C, and efficiently expressed IL-24-iRGD with the isopropyl-β-D-thiogalactoside (IPTG) inducer at a concentration of 1 mmol/l. Following a 10-h induction period, the bacteria were harvested, resuspended in phosphate-buffered sodium (pH 6.8) and lysed by ultrasonication in ice-water at 4 °C for 10 min. Centrifugation was performed at 16,000 ×*g* for 20 min at 4 °C. Urea (8 mol/l) was used to denature the undissolved proteins. The proteins were then purified by Co-NTA His Bind resin chromatography (TALON Metal Affinity Resin; cat. no. 635502; Takara Biotechnology, Co., Ltd., Dalian, China), and eluted with 250 mmol/l imidazole. Renaturation of IL-24-iRGD protein was performed by dialyzing against a low concentration of urea solution (4–0 mol/l). Finally, the purified proteins were dialyzed against water and stored at −80 °C following lyophilization. Samples were analyzed by 15% SDS-PAGE analysis (Fig. 1B).

2.4. Western blot analysis to determine the specificity of anti-IL-24 antibodies

Western blotting was used to analyze the specificity of anti-IL-24 antibodies (Fig. 1C). IL-24-iRGD and IL-24 (PeproTech, cat. no. 96-200-35, USA) were electrophoresed on a 15% SDS-PAGE gel and then transferred to a nitrocellulose membrane (Merck KGaA). The membrane was blocked with 5% bovine serum albumin (BSA) for 1 h at room temperature (RT), washed with phosphate-buffered saline + Tween 20 (PBST) and probed with a rabbit anti-human IL-24 antibody (dilution, 1:500; cat. no. ab115207; Abcam, Cambridge, MA, USA) for 1 h at 37 °C. This was followed by incubation with a horseradish peroxidase (HRP)-conjugated goat anti-rabbit IgG secondary antibody (dilution, 1:500; cat. no. VA001; Vicmed Biotech Co., Ltd., Xuzhou, China) for 1 h at RT. The reaction was completed with 0.05% 3,3′-diaminobenzidine (DAB) and 0.012% H_2O_2 for 15 min at 37 °C (Fig. 1C).

2.5. ELISA for bioactivity assay

In order to test the bioactivity of IL-24-iRGD *in vitro*, enzyme-linked immunosorbent assay (ELISA) was used to measure the induction of IL-6, tumor necrosis factor-α (TNF-α), and interferon-γ (IFN-γ) from human peripheral blood monocytes (PBMCs) by IL-24-iRGD. Briefly, 96-well flat-bottomed ELISA plates (Costar, USA) were coated with 100 μl/well of PBMC (5×10^6/ml) in RPMI-1640, with 10% fetal calf serum and incubated with 10 μg/ml of IL-24-iRGD or IL-24 for 48 h at 37 °C. After that, the supernatant were collected. Besides, enzyme strips (Keygen Kit, Nanjing KeyGen Biotech, China), which respectively precoated with anti-human IL-6, TNF-α, and IFN-γ monoclonal antibody (McAb), were used as instructions. Strips were incubated with 100 μl/well of the supernatant for 90 min at 37 °C. After washed 5 times, they were incubated with biotin-conjugated goat anti-human IgG for 1 h at 37 °C. Then, they were incubated with 100 μl HRP-conjugated streptavidin for 30 min at RT, and 100 μl of TMB for 15 min in dark, respectively. The reaction was terminated with stop buffer and finally, the OD450 value was measured using an ELISA reader (Bio-Rad, Hercules, CA, USA) (Fig. 2).

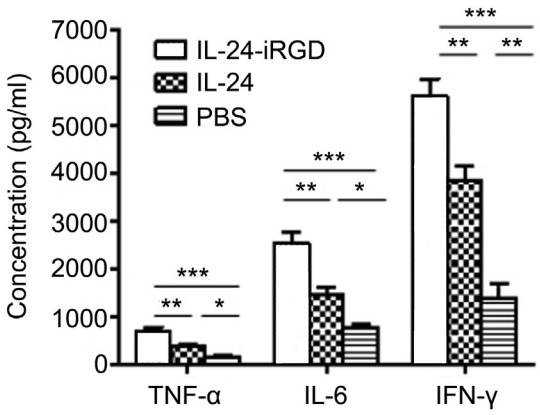

Fig. 2. Analysis of the bioactivity of IL-24-iRGD. Effects of induction of cytokines on PBMC was assessed by ELISA. Human TNF-α, IL-6, and IFN-γ were quantitated in culture supernatants by ELISA kit according to the manufacturer's instruction. Data are presented as the mean ± standard deviation (S.D.) from three independent experiments (n = 3). $^{*}P < 0.05$, $^{**}P < 0.01$ and $^{***}P < 0.001$, as indicated.

2.6. Flow cytometry

A total of 1×10^6 A549 cells were digested with accutase-enzyme cell detachment medium (cat. no. 85-00-4555-56; eBioscience) for 5 min at 37 °C and washed with phosphate-buffered saline (PBS) twice. And then, cells were incubated with 5 μl fluorescent-labeled antibodies diluted in 100 μl PBS for 30 min, RT. The cells were then washed, resuspended and analyzed using flow cytometer (FACSCanto II; BD Biosciences, Franklin Lakes, NJ, USA). The Annexin V-fluorescein isothiocyanate (FITC)-conjugated mouse anti-human integrin αvβ3 antibody (cat. no. MAB1976F) and integrin αvβ5 antibodies (cat. no. MAB1961F) were purchased from Merck KGaA. The matched isotype control antibody, FITC-conjugated mouse IgG1κ was purchased from eBioscience, Inc. (cat. no. 11-4714-42; San Diego, CA, USA). The phycoerythrin (PE)-conjugated mouse anti-human NRP-1 antibody was purchased from Miltenyi Biotec, Inc. (cat. no. 130-098-876; Cambridge, MA, USA). The flow cytometry results were analyzed using flowjo software 7.6.1 (Fig. 3).

2.7. CCK-8 method for cytopathic assay

In order to assess its cytopathic effect on inhibiting tumor cells growth of IL-24-iRGD *in vitro*, cell counting kit-8 (CCK-8, Tiagen, Beijing, China) was used as instructions. A549 and NHLF cells (5×10^3/well) were plated in 96-well plates and treated with 10–70 μg/ml of IL-24-iRGD or IL-24 at 37 °C the next day. Incubation for 24 h, 48 h, and 72 h, CCK-8 (10 μl) was added to each well and the cells were incubated for 4 h. Finally, the OD450 value was measured using an ELISA reader (Bio-Rad, Hercules, CA, USA) (Fig. 4). We set three replicate wells per assay, and each experiment was repeated twice.

2.8. Cell apoptosis assessment

Annexin V-FITC/propidium iodide (PI) staining was used for cell apoptosis assay. Briefly, A549 and NHLF cells were cultured in 24-well plates at 37 °C, 5% CO_2, and treated with 70 μg/ml of IL-24-iRGD or IL-24 for 48 h and then washed twice with PBS. 500 μl Binding Buffer, 5 μl Annexin V-FITC and 5 μl PI was added to the cells in turn and incubated for 30 min, RT. Pictures of the samples were taken under a fluorescence microscope (Fig. 5A). The integrated optical density (IOD) index for each selected area was analyzed using Image-Pro Plus 6.0 software (Fig. 5B and C).

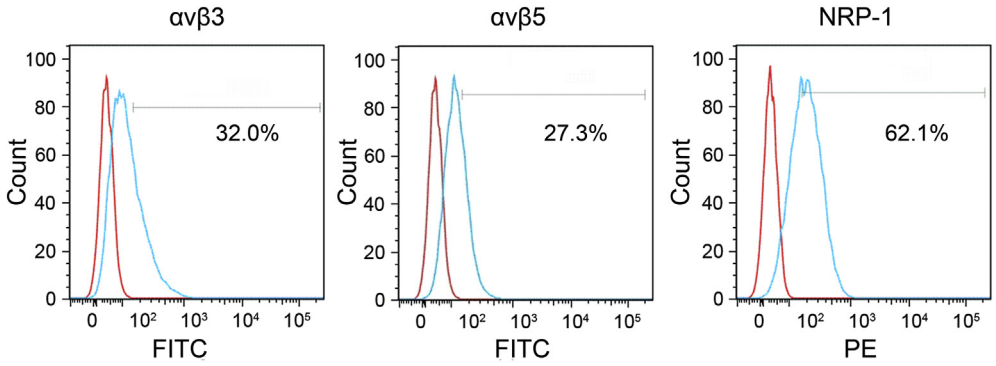

Fig. 3. Expression analysis of integrin αvβ3 and αvβ5, and NRP-1 in A549 cells by flow cytometry. Red line represented the isotype, and the blue line represented the sample. The flow cytometry results were analyzed using flowjo software 7.6.1. NRP-1, neuropilin-1. (For interpretation of the references to color in this figure legend, the reader is referred to the web version of this article.)

2.9. Evaluation of tumor tissue penetration

A549 cells (1×10^6 cells diluted in 100 µl PBS) were subcutaneously injected into the right flank of 8 mice. Tumor-bearing nude mice were randomly divided into IL-24 or IL-24-iRGD groups (n = 4/group) at ~4 weeks following injection of A549 cells. Assignment of mice into each group was based on tumor size to ensure there were no statistically significant differences in tumor volume between the groups at the time treatment commenced. Mice in each group received an intravenous injection into caudal vein of 10 µg/g IL-24 or 10 µg/g IL-24-iRGD, respectively. At 2 h and 6 h following treatment the tumors were excised, paraffin-embedded and divided into 4-µm sections (undertaken by pathology department of the affiliated hospital of Xuzhou Medical University, Jiangsu, China). The degree of protein penetration in tumors was analyzed by immunofluorescence. Briefly, tissue sections were stained with a primary rabbit anti-human IL-24 antibody (dilution, 1:100; cat. no. ab115207, Abcam) overnight at 4 °C, prior to staining with a DyLight 549-conjugated goat anti-rabbit IgG (H + L) secondary antibody (dilution, 1:100; cat no. E032320, Earthox Life Sciences, Millbrae, CA, USA) at 37 °C for 1 h. The sections were then stained with 50 µl DAPI at 37 °C for 15 min. Tissue sections were analyzed and photographed using a fluorescence microscope (DS-Ri1 Digital Camera; Nikon Corporation, Tokyo, Japan) (Fig. 6).

2.10. Tumor model and treatment in vivo

A549 cells (1×10^6 cells diluted in 100 µl PBS) were subcutaneously injected into the right flank of 18 mice. Tumor-bearing mice were randomly assigned to the following 3 treatment groups (n = 6/group) at ~4 weeks following injection of A549 cells: IL-24, IL-24-iRGD and PBS. Mice were assigned into groups based on tumor size to ensure there were no statistically significant differences in tumor volume among the groups at the time that treatment commenced. They were injected with 10 µg/g IL-24, 10 µg/g IL-24-iRGD or 100 µl PBS in the tail vein every 3 days and meanwhile, the tumor volume and the weight of nude mice was determined (Fig. 7). The volume of the tumors was calculated from two diameter measurements using a digital vernier caliper and the following formula: Tumor volume = (length × width^2) / 2. Following 5 rounds of treatment, all of the mice were sacrificed by neck death for tumor weight analysis. The tumor tissues were saturated in 10% formalin solution for 48 h, RT.

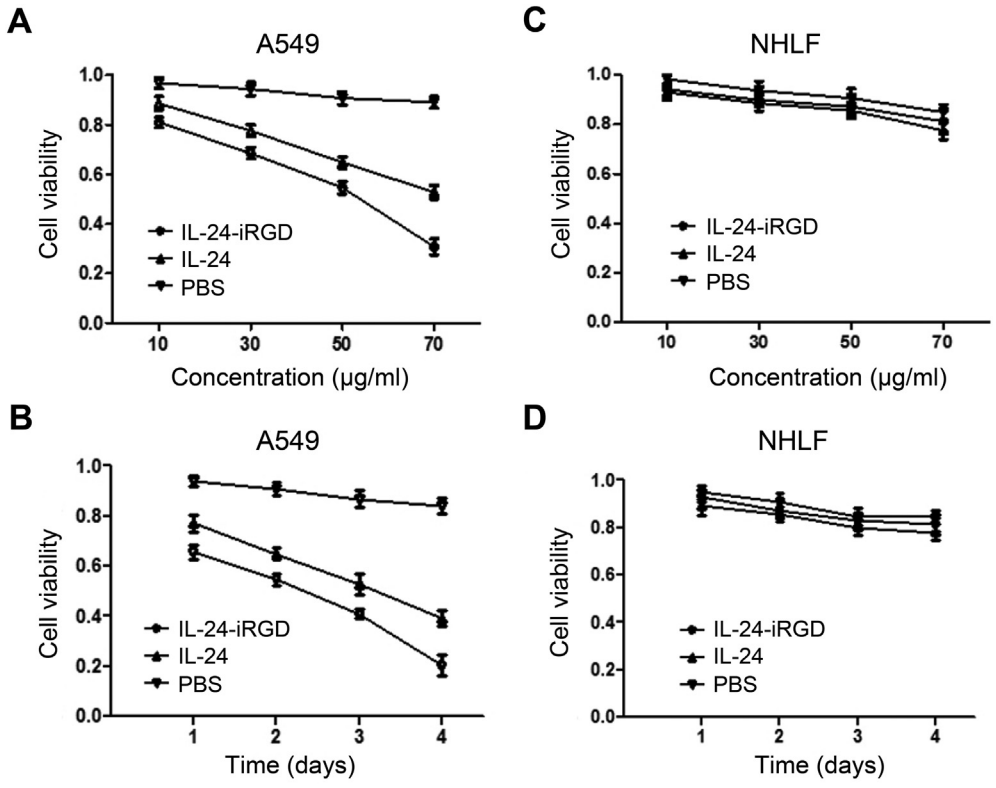

Fig. 4. Inhibition and cytopathic effect of IL-24-iRGD on cell growth. A549 and NHLF cells were treated with the dose of 10–70 µg/ml of IL-24-iRGD or IL-24 (A and C), and the time of 24 h, 48 h and 72 h (B and D). On days 1, 2, 3 and 4 post-administration, cells were subjected to the CCK-8 assay. Data are presented as the mean ± standard deviation (S.D.) from three independent experiments (n = 3).

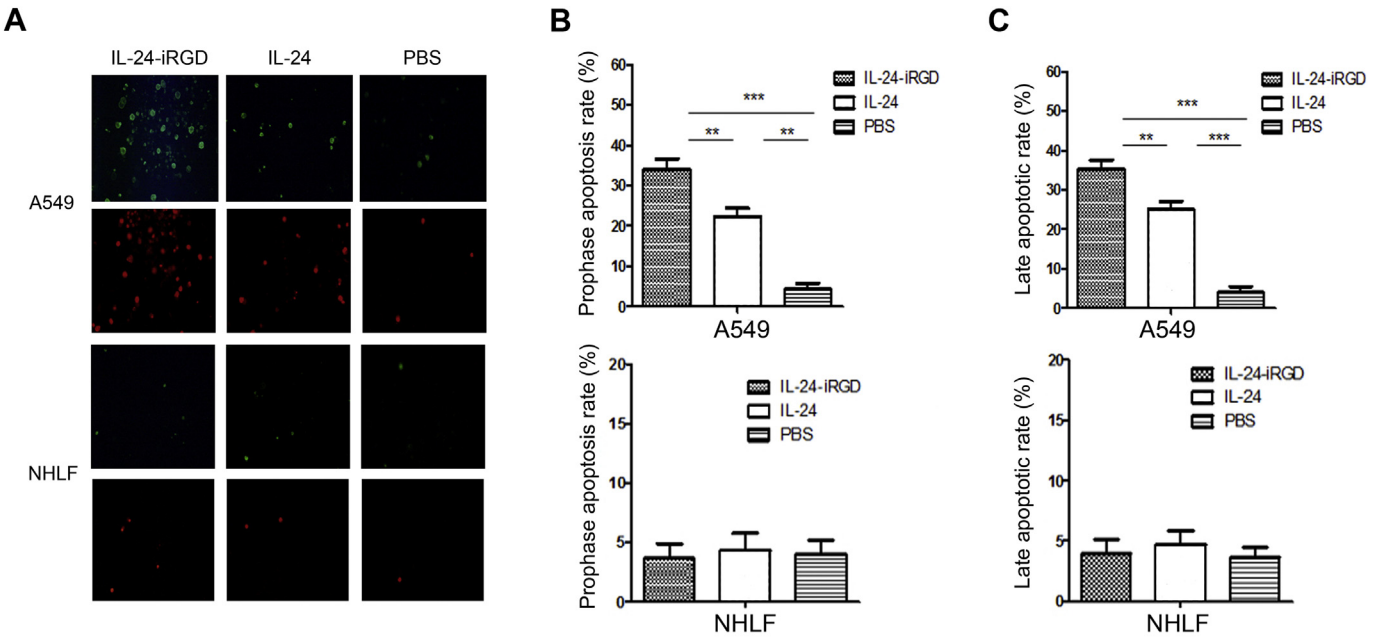

Fig. 5. Cell apoptosis analysis by Annexin V-FITC and PI staining. (A) Representative photomicrographs showing Annexin V-FITC staining (the green) for prophase apoptosis and PI staining (the red) for advanced stage apoptosis in A549 and NHLF cells treated with IL-24-iRGD, IL-24 and PBS (magnification, ×200). (B) Quantitative representation of the proportion of prophase apoptosis analyzed in A549 and NHLF. (C) Quantitative representation of the proportion of advanced stage apoptosis analyzed in A549 and NHLF. Data are presented as the mean ± standard deviation (S.D.). $^{*}P < 0.05$, $^{**}P < 0.01$ and $^{***}P < 0.001$, as indicated. (For interpretation of the references to color in this figure legend, the reader is referred to the web version of this article.)

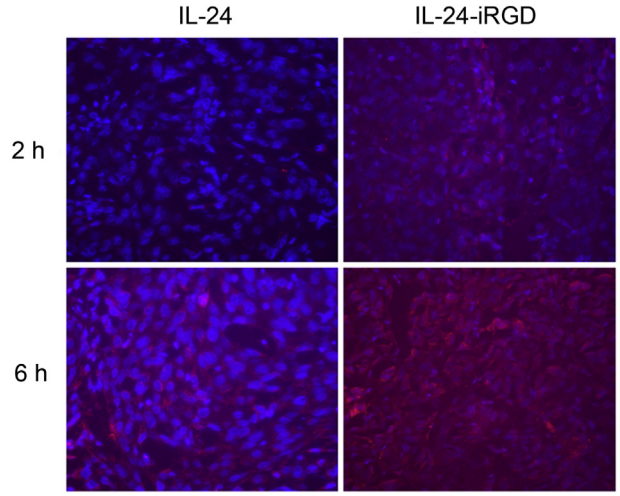

Fig. 6. Analysis of the penetration of IL-24 in A549 tumor tissues. A total of 10 μg/g of IL-24 or IL-24-iRGD was injected into the tail vein of A549-bearing mice. After 2 and 6 h of treatment, the penetration of IL-24 in A549 xenograft tumors was detected by immunofluorescence staining. Red staining indicates IL-24 protein and blue represents DAPI staining, indicating the nucleus. n = 4; magnification, ×400. DAPI, 4′,6-diamidino-2-phenylindole. (For interpretation of the references to color in this figure legend, the reader is referred to the web version of this article.)

2.11. TdT-mediated dUTP nick end labeling (TUNEL) assay

Tumor tissue sections from mice in each treatment group were formalin-fixed, paraffin-embedded and divided into 4-μm sections using the aforementioned procedures. The number of apoptotic cells was detected using an *In Situ* Cell Death Detection kit (cat. no. 11684817910; Sigma-Aldrich; Merck KGaA) according to the manufacturer's instructions. The number of TUNEL-positive cells was counted in five fields of view selected at random for each tumor tissue sample (magnification, ×400), and the apoptotic index in each field was calculated as the percentage of TUNEL-positive cells relative to 100 randomly selected cells. It was undertaken by fluorescent inverted microscope (IX83, Olympus). The IOD index for each selected area was analyzed using Image-Pro Plus 6.0 software (Fig. 8).

2.12. Expression of cleaved caspase-3 in tumor tissues

The expression of cleaved caspase-3 was analyzed by immunohistochemical analysis, and the experiments were performed using a streptavidin-peroxidase kit, according to the manufacturer's instructions (cat. no. SP9000; ZSGB-BIO, Beijing, China). Briefly, tumor tissues that had been formalin-fixed, were paraffin-embedded and divided into 4-μm sections. The tissue sections were then incubated with a rabbit anti-human cleaved caspase-3 antibody (dilution with PBS, 1:100; cat. no. ab13847, Abcam) overnight at 4 °C. Following incubation with solutions B and C at 37 °C for 30 min respectively, the sections were stained with 50 μl DAB for 30s and hematoxylin for 4 min, RT. All sections were observed and photographed with a fluorescence microscope (Fig. 9). To determine the IOD index of cleaved caspase-3, five representative fields of view that were positive for cleaved caspase-3 staining were examined for each tumor section (magnification, ×400). The IOD index for each selected area was analyzed using Image-Pro Plus 6.0 software (Media Cybernetics, Inc., Rockville, MD, USA).

2.13. Cytopathic effect assessment

Hematoxylin and eosin (H&E) staining was used to assess the cytopathic effect of IL-24-iRGD. Briefly, tissues of internal organs were fixed with 4% paraformaldehyde, embedded in paraffin and cut in 4-mm sections. The slides were deparaffinized with alcohol, washed with distilled water, stained with hematoxylin for 5 min, washed with distilled water, restained with eosin for 2 min and then decolorized with distilled water. After dehydration, the slides were made transparent with two treatments of xylene for 1 min each. Finally, the slides were mounted with neutral gum to be observed under the microscope (Fig. 10).

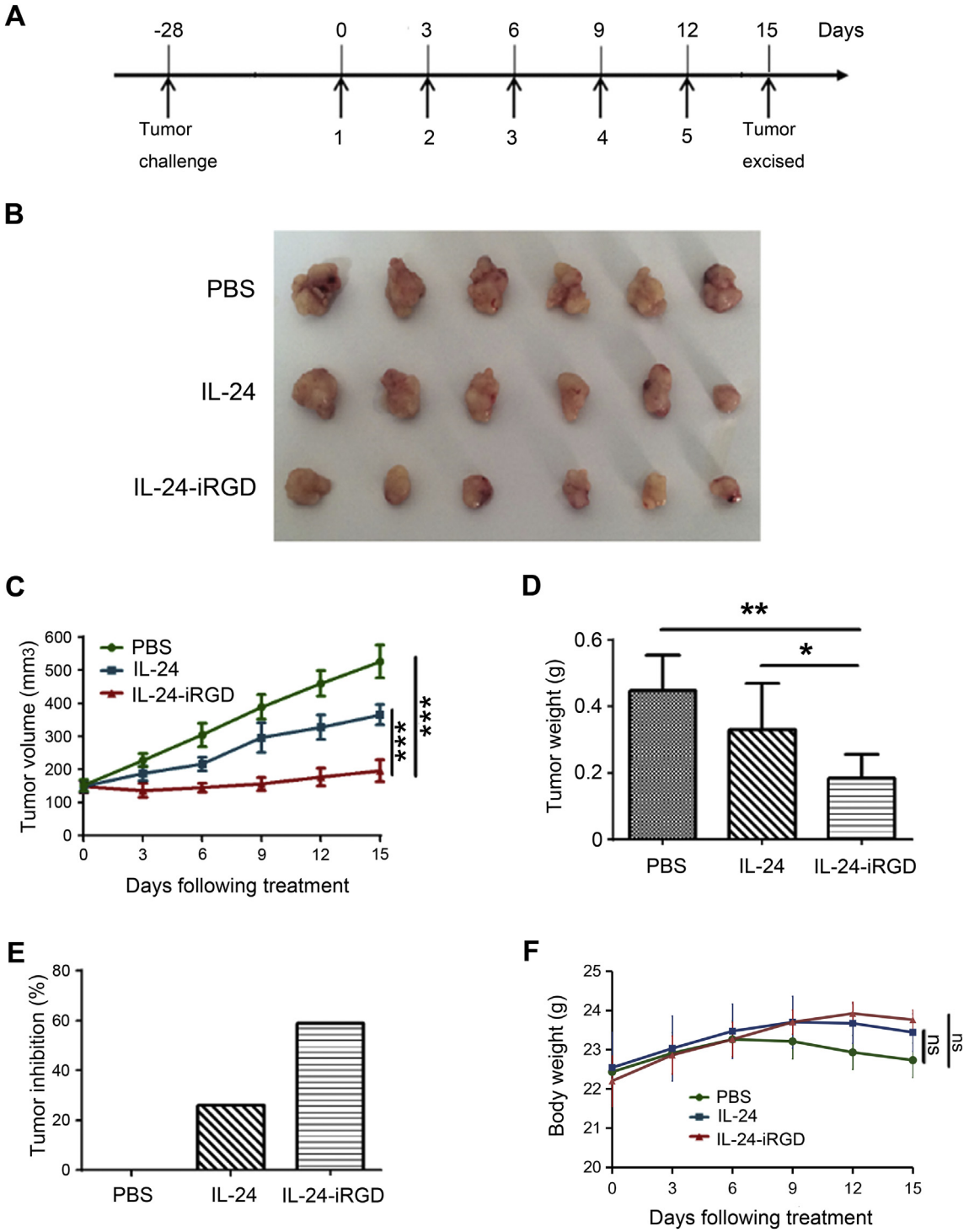

Fig. 7. Therapeutic efficacy of IL-24-iRGD *in vivo*. (A) Establishment of the A549-mouse tumor model and treatment regimen. (B) Solid tumors excised from mice injected with PBS, IL-24 or IL-24-iRGD (n = 6/group). (C) Tumor volume over the course of treatment. Tumor volume was measured once every three days until day 15. (D) Comparison of the average tumor weight in each group at the end of treatment. (E) Tumor inhibition rate of IL-24 and IL-24-iRGD. Tumor inhibition (%) = $(W_{PBS}\text{-}W_{IL\text{-}24\text{-}iRGD})/W_{PBS}$. (F) Body weights of mice in each group over the course of treatment (n = 6/group). Data are expressed as the mean ± standard deviation. $^{*}P < 0.05$, $^{**}P < 0.01$ and $^{***}P < 0.001$, as indicated. IL-24, interleukin-24; PBS, phosphate-buffered saline; ns, not significant.

2.14. Statistical analysis

Quantitative data are presented as the mean ± standard deviation (SD). An independent samples *t*-test was used to compare two groups. $P < 0.05$ was considered to indicate a statistically significant difference.

3. Results

3.1. Preparation of IL-24-iRGD

The pET19b-IL-24-iRGD vector was generated to express IL-24-iRGD (Fig. 1A). IL-24-iRGD (molecular weight, 21 kDa) was efficiently expressed in recombinant BL21 *E. coli*, and purified by affinity resin

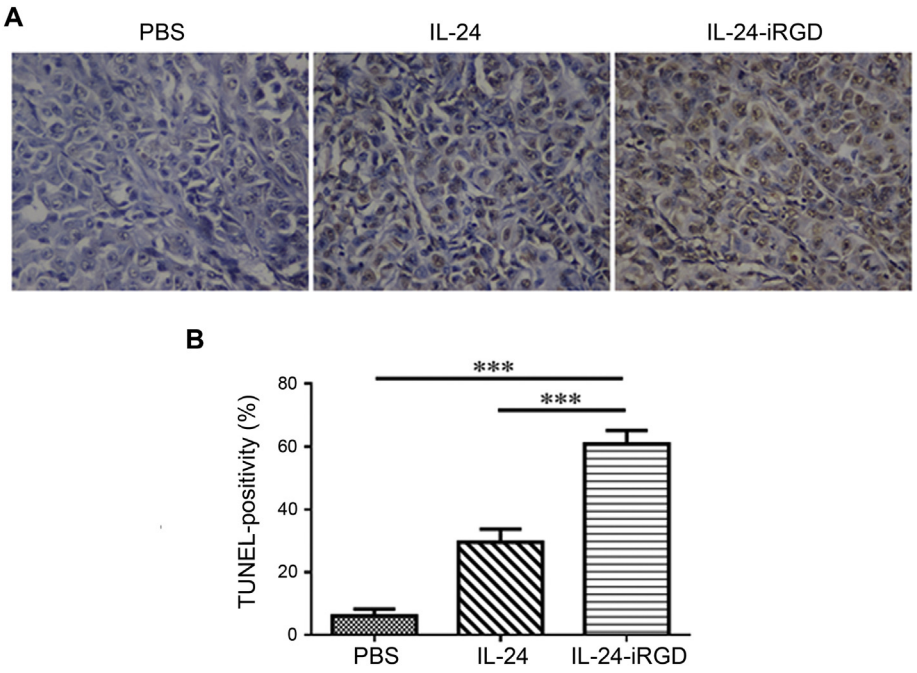

Fig. 8. TUNEL analysis of A549 xenograft tumor tissues. (A) Representative microscope images of TUNEL-stained tumor tissue sections derived from mice treated with PBS, IL-24 or IL-24-iRGD. TUNEL-positive nuclei are stained brown, and TUNEL-negative nuclei are stained blue (n = 6/group; magnification, ×400). (B) Quantitative analysis of TUNEL-staining in each group. The percentage of TUNEL-positive cells was counted from 100 tumor cells selected at random in each tissue section and 5 sections were counted per tumor (n = 6). Data are presented as the mean ± standard deviation. ***P < 0.001, as indicated. TUNEL, TdT-mediated dUTP nick end labeling; PBS, phosphate-buffered saline; IL-24, interleukin-24. (For interpretation of the references to color in this figure, the reader is referred to the web version of this article.)

chromatography to approximate homogeneity on a 15% SDS-PAGE gel (Fig. 1B). In addition, IL-24 and IL-24-iRGD were analyzed by western blotting using an anti-IL-24 antibody to verify the correct preparation of the proteins (Fig. 1C).

3.2. ELISA for bioactivity assay

The bioactivity of IL-24-iRGD to induce the cytokines from PBMC was assayed by ELISA. As shown in Fig. 2, the amount of IL-6, TNF-α, and IFN-γ produced by IL-24-iRGD stimulating PBMC were significantly higher than PBS group, which is much different between the two groups ($P < 0.05$). The results showed that IL-24-iRGD could effectively induce the production of IL-6, TNF-α, and IFN-γ from PBMC.

3.3. Expression of αvβ3, αvβ5 and NRP-1 in A549

To verify whether A549 was suitable for this experiment, expression of αvβ3, αvβ5 and NRP-1 in A549 cells was confirmed by flow cytometry analysis. As shown in Fig. 3, the positive expression rates of αvβ3, αvβ5, and NRP-1 were 32.0%, 27.3%, and 62.1%, respectively. These results demonstrated that the A549 cell line may be useful for the establishment of a human NSCLC model to study the effects of IL-24-iRGD.

3.4. CCK-8 assay

Here, CCK-8 assay was used to assess its cytopathic effect on inhibiting tumor cells growth of IL-24-iRGD *in vitro*. We compared the results of the treatments with the time of 24 h, 48 h and 72 h, and the

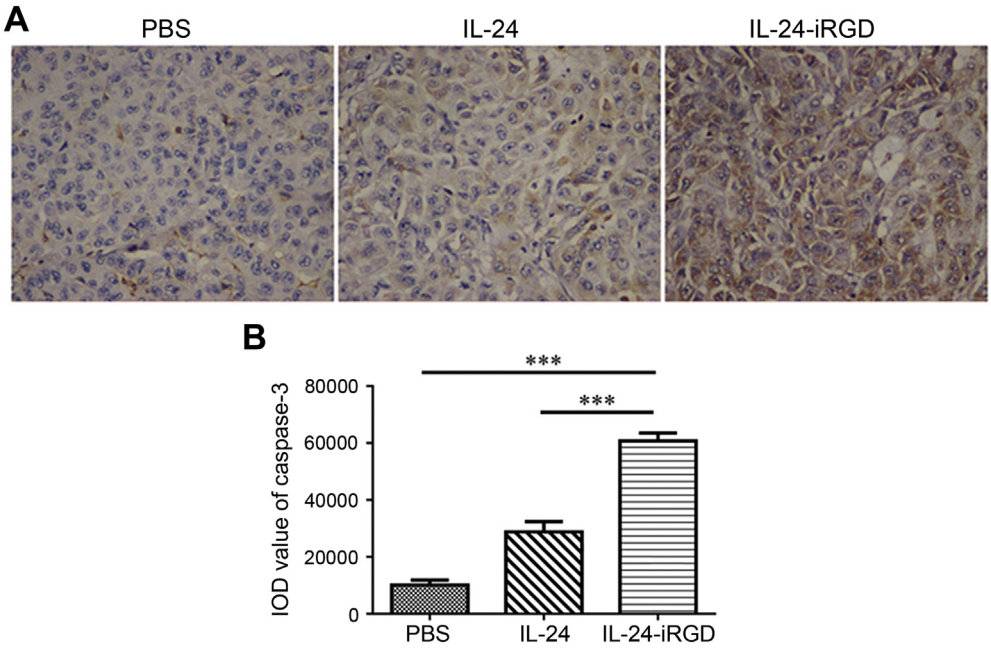

Fig. 9. Caspase-3 analysis of A549 xenograft tumor tissues. (A) Expression of cleaved caspase-3 in A549 tumor xenograft tissues following treatment with PBS, IL-24 or IL-24-iRGD. Brown staining indicates positive cleaved caspase-3 expression and blue staining indicates cell nuclei. Representative images from each group are shown (n = 6/group; magnification, ×400). (B) Quantitative analysis of cleaved caspase-3 staining in each treatment group. A total of 5 fields of view for each tumor tissue section were selected at random. IOD values of positively stained regions were calculated using Image-Pro Plus software (n = 6/group). Data are expressed as the mean ± standard deviation. ***P < 0.001, as indicated. PBS, phosphate-buffered saline; IL-24, interleukin-24; IOD, integrated optical density. (For interpretation of the references to color in this figure legend, the reader is referred to the web version of this article.)

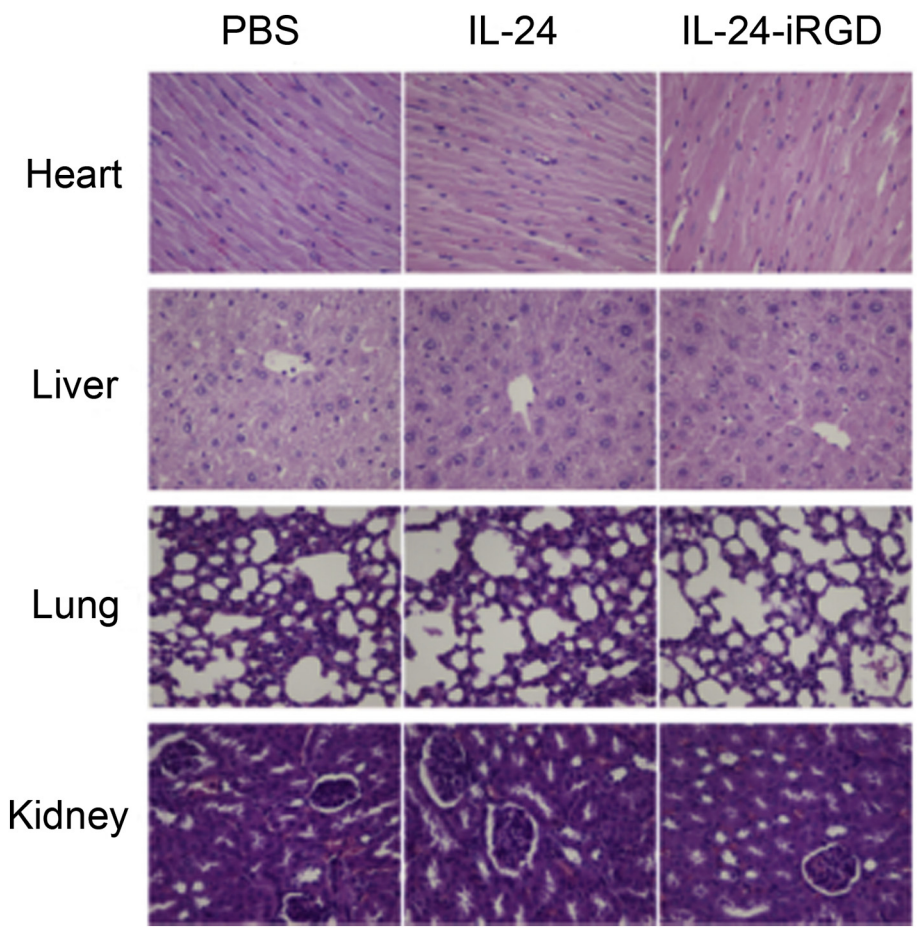

Fig. 10. H&E analysis of internal organs of treated mice. To test whether the tissue of internal organs was injured when IL-24-iRGD was administrated *in vivo*, the heart, liver, lung, and kidney of mice were excised and analyzed by H&E staining (magnification, ×400).

dose of 10–70 μg/ml of IL-24-iRGD or IL-24. As shown in Fig. 4, CCK-8 results demonstrated that both of IL-24-iRGD and IL-24 could inhibit tumor cell (A549) growth *in vitro*, and result in dose-time dependence (Fig. 4A and B), while they had no effect on normal cell line NHLF (Fig. 4C and D). Besides, the treatment of IL-24-iRGD had higher inhibition ability than the other groups. The data showed that IL-24-iRGD inhibited A549 cell proliferation effectively ($P < 0.05$).

3.5. Apoptosis by Annexin V-FITC/PI staining

Besides, annexin V-FITC/PI staining was used for cell apoptosis assay *in vitro* and the pictures were taken under a fluorescence microscope (Fig. 5A). Fig. 5B showed the results of annexin V-FITC staining, in which the green representing prophase apoptotic cells, and Fig. 5C showed the results of PI staining, in which the red representing advanced stage apoptotic cells. The results of annexin V-FITC/PI staining suggested that IL-24-iRGD could effectively induce tumor cell (A549) apoptosis *in vitro* ($P < 0.001$), but have no effect on normal cell line NHLF.

3.6. Tumor tissue penetration

In order to confirm the *in vivo* effects of the tumor-penetrating peptide, iRGD, and examine the expression of IL-24 in tumor tissues, we developed a BALB/c nude mouse model using the human A549 NSCLC cell line. The penetration of IL-24 into tumors was determined by immuno-fluorescence staining. As shown in Fig. 6, IL-24 displayed modest binding to the surface of the tumor tissue following injections at 2 h and 6 h, whereas IL-24-iRGD bound strongly, and even penetrated, several cell layers into the tumor tissue.

3.7. Therapeutic efficacy of IL-24-iRGD against A549 in vivo

To examine the therapeutic efficacy of IL-24-iRGD, the A549 mouse xenograft tumor model was first established. A schematic of the tumor model and treatment of mice was shown in Fig. 7A. The rate of tumor growth in the IL-24-iRGD group was reduced when compared with the IL-24 group, and the tumor volume of the IL-24-iRGD group was significantly reduced when compared with the PBS ($P < 0.001$) and IL-24 groups ($P < 0.001$; Fig. 7B and C). These observations were confirmed by an analysis of the tumor weight in each group (Fig. 7D). The rate of tumor growth inhibition was then analyzed further. Tumor inhibition (%) was calculated by the subtraction and division of average weight of tumors in PBS group and IL-24 or IL-24-iRGD group. At the end of the experiment, tumors from mice in the IL-24 group and the IL-24-iRGD group exhibited growth inhibition rates of 26.2% and 59.1%, respectively (Fig. 7E). Notably, the body weight of mice in each experimental group was not significantly different (Fig. 7F). These results demonstrated that iRGD efficiently enhanced the therapeutic efficacy of IL-24 in human A549 NSCLC cells *in vivo*.

3.8. TUNEL analysis

Next, cancer cell death of treated mice was analyzed by TUNEL staining. As shown in Fig. 8, tumors from mice in the IL-24-iRGD group exhibited significantly stronger TUNEL staining (the brown) when compared with tumors from mice treated with PBS or IL-24, which indicated substantial cancer cell death in the IL-24-iRGD-treated tumors

($P < 0.001$).

3.9. Expression of cleaved caspase-3 in tumor tissues

In addition, to assess and verify the apoptosis, the expression of cleaved caspase-3 was analyzed by immunohistochemical staining. Caspase-3 is a key apoptosis regulatory protein of the tumor cell death pathway [9]. The results of Fig. 9 revealed a significant increase in cleaved caspase-3 expression in the tumor tissues from mice in the IL-24-iRGD group when compared with the PBS and IL-24 groups ($P < 0.001$).

3.10. H&E analysis

Finally, to assess the cytopathic effect on mice of IL-24-iRGD, the slides of heart, liver, lung, and kidney of treated mice were analyzed by H&E staining. As shown in Fig. 10, there were no significant difference in the PBS, IL-24, or IL-24-iRGD groups. These data showed that, IL-24-iRGD was safe to these organs of the mice.

4. Discussion

The aim of the present study was to assess the use of iRGD peptide as a tool for improving the delivery and therapeutic efficacy of IL-24 treatment. The results demonstrated that it enhanced the accumulation and therapeutic efficacy of IL-24 in mouse NSCLC xenograft tumors, which were established using the A549 cell line that exhibited high expression levels of αvβ3, αvβ5 and NRP-1. In addition, the results demonstrated that the IL-24-iRGD protein induced apoptosis, accelerated cell death and inhibited tumor cell growth to a greater extent than IL-24 treatment alone. This was considered to be due to the efficient iRGD-mediated increase in the tumor penetration ability of IL-24 in human A549 NSCLC tumors.

Previous studies have confirmed that IL-24 is a multi-faceted killer of numerous cancer cells that has shown great clinical benefit in patients [9]. The apoptotic pathways by IL-24 causes cell death in tumor cells are not fully understood; however, current evidence suggests an inherent complexity and an involvement of proteins important for the onset of growth inhibition and apoptosis, including Bcl-2, bax, and caspase [9,21]. It is revealed that IL-24 induces Bcl-2 S-denitrosylation, results in its ubiquitination and subsequent caspase protease family activation, as a consequence, apoptosis susceptibility [21]. In this study, IL-24 triggered the activation of caspase-3, and a significant increase in cleaved caspase-3 expression in the tumor tissues from mice in the IL-24-iRGD group was shown in Fig. 9.

Sieger et al. demonstrated that the tumor suppressor activity of IL-24 was mediated by the expression of intracellular proteins in NSCLC cells [22]. It is thought that penetration through the vascular wall and into the tumor parenchyma against the elevated interstitial pressure in tumors, remains a major challenge for improving the therapeutic efficacy of the majority of clinical drugs [17]. Research investigating IL-24 as an anti-cancer treatment has employed adenoviruses as carriers for transfecting cancer cells with the IL-24 gene, and IL-24 is a well-studied cytokine established as a therapeutic in a wide-array of cancers upon delivery as a gene therapy [21,22]. This method has demonstrated satisfactory anti-cancer effects; however, the adenovirus carriers may not be safe for clinical use. In 2016, Zhang et al. [23] reported the use of a transactivator of the transcription (TAT 47-57) from human immunodeficiency virus (HIV) type 1 as a carrier to deliver the IL-24 recombinant protein into cells. The TAT peptide has been demonstrated to deliver various biological molecules, including proteins, DNA and RNA, into almost all tissues and cell types, and even penetrates the blood-brain barrier [23]. However, the high efficiency of penetration into virtually all tissues and cells poses a great risk to human health. It may be considered that the indistinguishableness of TAT penetration could cause serious problems of the brain and other healthy organs.

In the present study, we explored the potential anti-cancer properties of IL-24 delivered as a recombinant protein. The iRGD peptide was used to overcome this tissue penetration problem, enhancing drug effects against tumors and reducing the drug dose in needed and in other healthy organs. It has been demonstrated that the tumor-penetrating ability of iRGD primarily depends on the expression of αvβ3, αvβ5 and NRP-1 in cancer cells [3,17]. The expression of integrins is largely restricted to tumors [17], and NRP-1 is overexpressed in a number of tumors [17,23]. We found that A549 was an eligible model for the present study, as it positively expresses αvβ3, αvβ5 and NRP-1 [3,4]. Flow cytometry analysis confirmed that αvβ3, αvβ5 and NRP-1, which mediate the tumor-penetration activity of iRGD, were overexpressed in the human A549 NSCLC cell line.

In the present study, immunofluorescence staining of A549 mouse xenograft tumor tissues revealed that IL-24-iRGD penetrated tumor tissues to a larger extent when compared with IL-24 treatment alone. In our study, treatment with IL-24-iRGD protein was associated with a significant reduction in tumor growth when compared with IL-24 monotherapy in the mouse with lung cancer models established with A549 cell lines. Therefore, the therapeutic efficacy of IL-24 was significantly enhanced by fusing this gene with iRGD in a murine NSCLC cancer model. Together, these studies confirm the effects of iRGD in enhancing the intratumoral dissemination and anticancer efficacy of IL-24 in NRP-1-overexpressing cancer models. To the best of the author's knowledge, the present study is the first to demonstrate the efficacy of IL-24-iRGD against human A549 NSCLC cells.

5. Conclusion

IL-24-iRGD enhanced the effect of IL-24 against A549 cells by inducing apoptosis and inhibiting tumor cell growth *in vitro* and *in vivo*. The mechanisms underlying the antitumor effects of IL-24-iRGD against NSCLCs were explored in a preliminary study. The results present a novel strategy for improving the efficacy of IL-24 antitumor therapy, which may be used for the clinical treatment of patients with NSCLC in the future.

Acknowledgements

The present study was supported by grants from the Natural Science Foundation of China (grant nos. 81372460, 81702499, 81773253 and 81872488), the Natural Science Foundation of Jiangsu Province (grant no. BK20161156, BK20161157, and BK20170266), the Social Development Project of Jiangsu Province (grant number SBE2018740637); the Natural Science Key Project of Jiangsu Provincial Department of Education (grant number 17KJA320011); and the Key Medical Subjects of Jiangsu Province, the Project of Invigorating Health Care through Science, Technology and Education (no. ZDXKA2016014).

References

[1] F. Bray, J. Ferlay, I. Soerjomataram, R.L. Siegel, L.A. Torre, A. Jemal, Global cancer statistics 2018: GLOBOCAN estimates of incidence and mortality worldwide for 36 cancers in 185 countries, CA Cancer J. Clin. 68 (6) (2018) 394–424.
[2] R.L. Siegel, K.D. Miller, A. Jemal, Cancer statistics, 2018, CA Cancer J. Clin. 68 (2018) 7–30.
[3] Q. Zhang, Y. Zhang, K. Li, H. Wang, H. Li, J. Zheng, A novel strategy to improve the therapeutic efficacy of gemcitabine for non-small cell lung cancer by the tumor-penetrating peptide iRGD, PLoS One 10 (2015) e0129865.
[4] Y. Zhang, J. Yang, M. Ding, L. Li, Z. Lu, Q. Zhang, et al., Tumor-penetration and antitumor efficacy of cetuximab are enhanced by co-administered iRGD in a murine model of human NSCLC, Oncol. Lett. 12 (2016) 3241–3249.
[5] S. Peters, A.A. Adjei, C. Gridelli, M. Reck, K. Kerr, E. Felip, Metastatic non-small-cell lung cancer (NSCLC): ESMO Clinical Practice Guidelines for diagnosis, treatment and follow-up, Ann. Oncol. 23 (Suppl 7) (2012) vii56–64.
[6] Z. Hai-Tao, L. Hui-Cheng, L. Zheng-Wu, G. Chang-Hong, A tumor-penetrating peptide modification enhances the antitumor activity of endostatin in vivo, Anti-Cancer Drugs 22 (2011) 409–415.
[7] T. Teesalu, K.N. Sugahara, E. Ruoslahti, Tumor-penetrating peptides, Front. Oncol.

3 (2013) 216.
[8] P.B. Fisher, Is mda-7/IL-24 a "magic bullet" for cancer? Cancer Res. 65 (2005) 10128–10138.
[9] P. Dent, A. Yacoub, H.A. Hamed, M.A. Park, R. Dash, S.K. Bhutia, et al., MDA-7/IL-24 as a cancer therapeutic: from bench to bedside, Anti-Cancer Drugs 21 (2010) 725–731.
[10] M.E. Menezes, S. Bhatia, P. Bhoopathi, S.K. Das, L. Emdad, S. Dasgupta, et al., MDA-7/IL-24: multifunctional cancer killing cytokine, Adv. Exp. Med. Biol. 818 (2014) 127–153.
[11] A.K. Pradhan, P. Bhoopathi, S. Talukdar, X.N. Shen, L. Emdad, S.K. Das, et al., Recombinant MDA-7/IL-24 suppresses prostate cancer bone metastasis through down regulation of the Akt/Mcl-1 pathway, Mol. Cancer Ther. (2018).
[12] J. Panneerselvam, J. Jin, M. Shanker, J. Lauderdale, J. Bates, Q. Wang, et al., IL-24 inhibits lung cancer cell migration and invasion by disrupting the SDF-1/CXCR4 signaling axis, PLoS One 10 (2015) e0122439.
[13] J. Yang, Q. Zhang, K. Li, H. Yin, J.N. Zheng, Composite peptide-based vaccines for cancer immunotherapy (Review), Int. J. Mol. Med. 35 (2015) 17–23.
[14] J.P. Xiong, T. Stehle, B. Diefenbach, R. Zhang, R. Dunker, D.L. Scott, et al., Crystal structure of the extracellular segment of integrin alpha Vbeta3, Science 294 (2001) 339–345.
[15] R. Bartolome, A. Pelaez-Garcia, I. Gomez, S. Torrres, M.J. Fernandez-Acenero, B. Escudero-Paniagua, et al., An RGD motif present in cadherin 17 induces integrin activation and tumor growth, J. Biol. Chem. 289 (50) (2014) 34801–34814.
[16] T. Teesalu, K.N. Sugahara, V.R. Kotamraju, E. Ruoslahti, C-end rule peptides mediate neuropilin-1-dependent cell, vascular, and tissue penetration, Proc. Natl. Acad. Sci. U. S. A. 106 (2009) 16157–16162.
[17] K.N. Sugahara, T. Teesalu, P.P. Karmali, V.R. Kotamraju, L. Agemy, O.M. Girard, et al., Tissue-penetrating delivery of compounds and nanoparticles into tumors, Cancer Cell 16 (2009) 510–520.
[18] G. De, J.K. Ko, T. Tan, H. Zhu, H. Li, J. Ma, Amphipathic tail-anchoring peptide is a promising therapeutic agent for prostate cancer treatment, Oncotarget. 5 (2014) 7734–7747.
[19] R. Chen, G.B. Braun, X. Luo, K.N. Sugahara, T. Teesalu, E. Ruoslahti, Application of a Proapoptotic Peptide to Intratumorally Spreading Cancer Therapy, Cancer Res. 73 (2012) 1352–1361.
[20] Y. Akashi, T. Oda, Y. Ohara, R. Miyamoto, T. Kurokawa, S. Hashimoto, et al., Anticancer effects of gemcitabine are enhanced by co-administered iRGD peptide in murine pancreatic cancer models that overexpressed neuropilin-1, Br. J. Cancer 110 (2014) 1481–1487.
[21] H. Tian, J. Wang, B. Zhang, J. Di, F. Chen, H. Li, et al., MDA-7/IL-24 induces Bcl-2 denitrosylation and ubiquitin-degradation involved in cancer cell apoptosis, PLoS One 7 (2012) e37200.
[22] K.A. Sieger, A.M. Mhashilkar, A. Stewart, R.B. Sutton, R.W. Strube, S.Y. Chen, et al., The tumor suppressor activity of MDA-7/IL-24 is mediated by intracellular protein expression in NSCLC cells, Mol. Ther. 9 (2004) 355–367.
[23] J. Zhang, A. Sun, R. Xu, X. Tao, Y. Dong, X. Lv, et al., Cell-penetrating and endoplasmic reticulum-locating TAT-IL-24-KDEL fusion protein induces tumor apoptosis, J. Cell. Physiol. 231 (2016) 84–93.